


Article

A Predictive Model for Wellbore Temperature in High-Sulfur Gas Wells Incorporating Sulfur Deposition

Qiang Fang ^{1,2,*} , Jinghong He ², Yang Wang ³, Hong Pan ³, Hongming Ren ³ and Hao Liu ²

¹ State Key Laboratory of Oil and Gas Reservoir Geology and Exploitation, Chengdu University of Technology, Chengdu 610059, China

² College of Energy (College of Modern Shale Gas Industry), Chengdu University of Technology, Chengdu 610059, China

³ PetroChina Southwest Oil and Gas field Company, Northeast Sichuan Gas District, Dazhou 635000, China

* Correspondence: fangqiang@cdut.edu.cn

Abstract: HSG (high-sulfur gas) reservoirs are prevalent globally, yet their exploitation is hindered by elevated levels of hydrogen sulfide. A decrease in temperature and pressure may result in the formation of sulfur deposits, thereby exerting a notable influence on gas production. Test instruments are susceptible to significant corrosion due to the presence of hydrogen sulfide, resulting in challenges in obtaining bottom hole temperature and pressure test data. Consequently, a WTD (wellbore temperature distribution) model incorporating sulfur precipitation was developed based on PPP (physical property parameter), heat transfer, and GSTP (gas–solid two-phase) flow models. The comparison of a 2.53% temperature error and a 4.80% pressure error with actual field test data indicates that the established model exhibits high accuracy. An analysis is conducted on the impact of various factors, such as production, sulfur layer thickness, reservoir temperature, and reservoir pressure, on the distribution of the wellbore temperature field and pressure field. Increased gas production leads to higher wellhead temperatures. The presence of sulfur deposits reduces the flow area and wellhead pressure. A 40% concentration of hydrogen sulfide results in a 2 MPa pressure drop compared to a 20% concentration. Decreased reservoir pressure and temperature facilitate the formation of sulfur deposits at the wellhead.



Citation: Fang, Q.; He, J.; Wang, Y.; Pan, H.; Ren, H.; Liu, H. A Predictive Model for Wellbore Temperature in High-Sulfur Gas Wells Incorporating Sulfur Deposition. *Processes* **2024**, *12*, 1073. <https://doi.org/10.3390/pr12061073>

Academic Editors: Paolo Blecich and Tomislav Mrakovčić

Received: 23 April 2024

Revised: 15 May 2024

Accepted: 20 May 2024

Published: 24 May 2024



Copyright: © 2024 by the authors. Licensee MDPI, Basel, Switzerland. This article is an open access article distributed under the terms and conditions of the Creative Commons Attribution (CC BY) license (<https://creativecommons.org/licenses/by/4.0/>).

Keywords: HSG reservoirs; sulfur deposition; WTD; predictive model; impact factors

1. Introduction

The ongoing expansion of natural gas exploration and development activities is driven by the desire for a clean, environmentally friendly, and high-calorific-value energy source. Of particular interest are HSG reservoirs, which are characterized by significant levels of hydrogen sulfide [1,2]. These reservoirs present unique challenges, as the presence of hydrogen sulfide not only poses environmental and safety risks but can also result in sulfur deposition under specific temperature and pressure conditions. In HSG wells, sulfur deposition transformation commonly takes place in regions of temperature fluctuation and pressure decrease, particularly in proximity to the wellhead [3–5]. The accumulation of sulfur can result in obstructions in pipelines, causing disruptions in gas flow and diminishing production output.

Comprehension of the impact of temperature and pressure on sulfur deposition can aid operators in optimizing the operational parameters, such as modifying the wellhead temperatures or adjusting the fluid dynamics conditions, to mitigate sulfur deposition, enhance production efficiency, and minimize operational downtime. The presence of HSG can lead to significant corrosion issues, with the rate and nature of corrosion being influenced by fluctuations in temperature and pressure [6,7]. The maintenance of precise temperature and pressure models is imperative for the evaluation and management of risks in HSG reservoirs, enabling the proactive identification and resolution of potential

problems and facilitating the development of efficient monitoring and control systems by operators.

The temperature and pressure distribution within wellbores has long been a focal point in the advancement of oil and gas field development, prompting numerous scholarly investigations. The initial research primarily focused on steady-state conditions, with Ramey pioneering a seminal numerical model for quasi-steady-state wellbore temperature fields [8]. Subsequent studies have yielded a wealth of findings that have been applied to diverse and intricate scenarios. Willhite, for instance, delved into the heat transfer mechanisms between the fluid components within tubing and the surrounding reservoir, culminating in the derivation of comprehensive heat transfer coefficient expression [9]. Raymond introduced the initial transient wellbore heat transfer model to address the temperature distribution in circulating drilling fluid [10]. Eickmeier et al. utilized the explicit finite difference method to discretize wellbores in both the radial and axial directions [11]. A fully implicit wellbore heat transfer numerical model was proposed by You, wherein the fluid energy equation was considered transient, while Ramey's steady-state heat transfer assumption was maintained for the wellbore section [12]. Dong et al. examined the distribution of wellbore temperature fields during volumetric fracturing, utilizing the Eickermeier model as a framework for their study [13].

In contrast to numerical models, analytical models offer the benefits of a rapid calculation speed and the absence of stability or convergence requirements. Consequently, scholars have introduced an analytical model for the wellbore temperature field under specific simplified conditions. Hasan and Kabir have extensively documented their work on an analytical model of the wellbore temperature field, focusing on enhancements to the dimensionless time function. Additionally, they have incorporated the relaxation distance into a transient equation for wellbore fluid and utilized the heat storage coefficient to represent the unsteady heat transfer characteristics [14–16].

In recent years, there has been continued emphasis on the investigation of the wellbore temperature field in academic research. Wang further contributed to this area of study by developing a mathematical model aimed at characterizing the distribution of temperature and pressure within wellbores, addressing the need for real-time monitoring of these parameters in gas injection wells [17]. Sun introduced a novel, comprehensive, and precise approach to forecasting wellbore temperature and pressure and the formation of hydrates [18]. Zheng introduced a coupling model that considers the relationship between wellbore temperature and pressure in a water-bearing gas well, examining the impact of the pipe diameter, gas production, gas–water ratio, and temperature and pressure fields in a high-water-bearing gas well [19]. An developed a numerical model to analyze the transient temperature–pressure coupling field in a small borehole [20]. Chen employed a wellbore heat transfer model to forecast transient temperature fluctuations, taking into account the influences of the drilling fluid characteristics, drill pipe eccentricity, rotation, and bit rock fracturing on annular temperature distributions [21].

When the concentration of elemental sulfur in the gas phase surpasses its solubility in natural gas with a high sulfur content, sulfur deposits may form in the wellbore. The solubility of elemental sulfur in gas is determined through various methods, including using experimental data, semi-empirical prediction models, thermodynamic models, and artificial neural network predictions. Numerous scholars have conducted extensive experimental studies to expand the scope of the experimental conditions, including the medium composition, pressure, and temperature. The medium component was expanded from a three-component system to a six-component system, with the experimental pressure increased to 137.9 MPa and the experimental temperature raised to 563 K [22–25].

Based on empirical data, scholars have conducted extensive research on theoretical prediction models of sulfur solubility in natural gas wellbores, resulting in the development of empirical correlation formulas with varying coefficients [26,27]. These formulas can effectively predict the sulfur solubility in sulfur-containing gas wellbores. Additionally, the current semi-empirical prediction model for sulfur solubility has demonstrated efficacy

in correlating elemental sulfur solubility under high-temperature and high-pressure conditions. Based on the principles of thermodynamic phase equilibrium, the dissolution of elemental sulfur in acidic natural gas can be conceptualized as an equilibrium problem between the gas and solid phases [28–30]. The solubility of sulfur is influenced by various factors, including pressure, temperature, and the concentration of temperamental components, making it challenging to establish a universal and simplified model for practical correlation. Given the superior precision of artificial neural network correlation functions in accounting for multiple influencing factors, numerous algorithms have been developed to address the issue of predicting sulfur solubility [31–33].

In summary, an in-depth analysis reveals that the current research on the distribution of temperature fields in wellbores and sulfur deposition is relatively extensive. However, there remains a lack of maturity in understanding the temperature fields of sulfur deposition in sulfur gas wells. This paper aims to delve deeper into the aforementioned issues, develop a predictive model tailored to temperature in the wellbores of HSG wells, assess the impact of key factors on the temperature field distribution, and offer insights for optimizing production systems and enhancing safety management in HSG reservoirs.

This study initially determined the PPP model, followed by the derivation of WTD and wellbore pressure models, as well as the integration of a sulfur solubility model. Subsequently, actual field test data were selected to validate and assess the accuracy of the models. Finally, the study analyzed the impacts of various key factors (such as gas production, sulfur layer thickness, HSC (hydrogen sulfide content), reservoir temperature, and reservoir pressure) on the distribution of wellbore temperature fields.

2. Methodology

2.1. PPP Models

2.1.1. Deviation Coefficient

In contrast to conventional gas reservoirs, HSG reservoirs exhibit more intricate and distinct fluid phase characteristics, resulting in a notably different gas deviation coefficient. The determination of this coefficient involves both experimental measurement and calculation methods. Due to the time-consuming and costly nature of the experimental measurement method, the empirical formula calculation method is typically employed.

Previous studies have shown that the DPR approach is closer to reality. Dranchuk, Purvis, and Robinson converted the deviation coefficient into a function of the contrast pressure and contrast temperature and derived an empirical formula with 8 constants in 1974 [34], as follows:

$$Z = 1 + \left(A_1 + \frac{A_2}{T_r} + \frac{A_3}{T_r^3} \right) \rho_r + \left(A_4 + \frac{A_5}{T_r} \right) \rho_r^2 + \left(\frac{A_5 A_6}{T_r} \right) \rho_r^5 + \frac{A_7}{T_r^3} \rho_r^2 (1 + A_8 \rho_r^2) \exp(-A_8 \rho_r^2) \quad (1)$$

$$\rho_r = 0.27 P_r / (Z T_r) \quad (2)$$

The values from A_1 to A_8 are shown in Table 1.

Table 1. DPR parameter values.

A_1	0.31506237	A_5	−0.61232032
A_2	−1.0467099	A_6	−0.10488813
A_3	−0.57832729	A_7	0.68157001
A_4	0.53530771	A_8	0.68446549

The inclusion of CO_2 and H_2S components in acidic gas influences the critical temperature and pressure of natural gas, resulting in an elevation of the gas deviation coefficient Z value and subsequent calculation inaccuracies. As such, it is imperative to adjust the

critical parameter properties for acidic natural gas. This study employs the Wichert–Aziz correction method [35] for this purpose.

$$\varepsilon = 15(M - M^2) + 4.167(N^{0.5} - N^2) \quad (3)$$

The critical temperature and pressure of each component should be correlated with the parameter ε , and the correction relationship for the critical parameter is outlined as follows.

$$T'_{ci} = T_{ci} - \varepsilon \quad (4)$$

$$p'_{ci} = p_{ci} T'_{ci} / T_{ci} \quad (5)$$

2.1.2. Viscosity

The viscosity of natural gas is calculated using the Dempsey method [36]:

$$\ln\left(\frac{\mu_g T_r}{\mu_1}\right) = B_0 + B_1 P_r + B_2 P_r^2 + B_3 P_r^3 + T_r(B_4 + B_5 P_r + B_6 P_r^2 + B_7 P_r^3) \\ + T_r^2(B_8 + B_9 P_r + B_{10} P_r^2 + B_{11} P_r^3) + T_r^3(B_{12} + B_{13} P_r + B_{14} P_r^2 + B_{15} P_r^3) \quad (6)$$

$$\mu_1 = (1.709 \times 10^{-5} - 2.062 \times 10^{-6} \gamma_g)(1.8T + 32) \\ + 8.188 \times 10^{-3} - 6.15 \times 10^{-3} \lg(\gamma_g) \quad (7)$$

The values from B_0 to B_{15} are shown in Table 2.

Table 2. Dempsey method parameter values.

B_0	−2.4621182	B_6	0.36037302	B_{12}	0.0839387178
B_1	2.97054714	B_7	−0.0104432413	B_{13}	−0.186408846
B_2	−0.286264054	B_8	−0.793385684	B_{14}	0.0203367881
B_3	0.00805420522	B_9	1.39643306	B_{15}	−0.000609579263
B_4	2.80860949	B_{10}	−0.149144925		
B_5	−3.49803305	B_{11}	0.00441015512		

Additionally, the viscosity of natural gas with an elevated sulfur content is frequently increased by the presence of non-hydrocarbon gases like H_2S . Therefore, it is essential to adjust for non-hydrocarbon effects when predicting the viscosity of HSG. The empirical method is used [37]:

$$\mu'_1 = \mu_1 + \mu_{N_2} + \mu_{CO_2} + \mu_{H_2S} \quad (8)$$

$$\mu_{N_2} = N_2 \cdot (8.48 \times 10^{-3} \lg(\gamma_g) + 9.59 \times 10^{-3})$$

$$\mu_{CO_2} = CO_2 \cdot (9.08 \times 10^{-3} \lg(\gamma_g) + 6.24 \times 10^{-3}) \quad (9)$$

$$\mu_{H_2S} = H_2S \cdot (8.49 \times 10^{-3} \lg(\gamma_g) + 3.73 \times 10^{-3})$$

2.1.3. Thermal Conductivity Coefficient

The thermal conductivity of sulfur exhibits temperature-dependent variability, with the thermal conductivity of solid sulfur demonstrating a gradual decrease as the temperature rises. The predictive equation describing the relationship between thermal conductivity and temperature for sulfur is as follows [38]:

$$\lambda = 0.8935 - 3.3347 \times 10^{-3} T + 4.1524 \times 10^{-6} T^2 \quad (10)$$

2.2. WTD Model

2.2.1. Equation of Heat Conduction

A thermal energy diagram for a microunit is depicted in Figure 1. In the absence of an internal heat source, the following, Equation (11), is derived in accordance with the principle of the conservation of energy.

$$q_x + q_y + q_z = q_{x+dx} + q_{y+dy} + q_{z+dz} + \frac{dE}{t} \quad (11)$$

The heat entering the microunit is

$$\begin{cases} q_x = -\lambda dydz \frac{\partial T}{\partial x} \\ q_y = -\lambda dx dz \frac{\partial T}{\partial y} \\ q_z = -\lambda dx dy \frac{\partial T}{\partial z} \end{cases} \quad (12)$$

The heat escaping from the microunit is

$$\begin{cases} q_{x+dx} = -\left[\lambda \frac{\partial T}{\partial x} + \frac{\partial}{\partial x} \left(\lambda \frac{\partial T}{\partial x} \right) dx \right] dy dz \\ q_{y+dy} = -\left[\lambda \frac{\partial T}{\partial y} + \frac{\partial}{\partial y} \left(\lambda \frac{\partial T}{\partial y} \right) dy \right] dx dz \\ q_{z+dz} = -\left[\lambda \frac{\partial T}{\partial z} + \frac{\partial}{\partial z} \left(\lambda \frac{\partial T}{\partial z} \right) dz \right] dx dy \end{cases} \quad (13)$$

The heat change inside the microunit is

$$\frac{dE}{t} = \rho c dx dy dz \frac{\partial T}{\partial t} \quad (14)$$

According to Equations (11)–(14):

$$\frac{\partial^2 T}{\partial x^2} + \frac{\partial^2 T}{\partial y^2} + \frac{\partial^2 T}{\partial z^2} = \frac{\rho c}{\lambda} \frac{\partial T}{\partial t} \quad (15)$$

For a wellbore, cylindrical coordinates are generally used, so Equation (15) can be converted into the following form:

$$\frac{\partial^2 T}{\partial r^2} + \frac{1}{r} \frac{\partial T}{\partial r} = \frac{\rho c}{\lambda} \frac{\partial T}{\partial \tau} \quad (16)$$

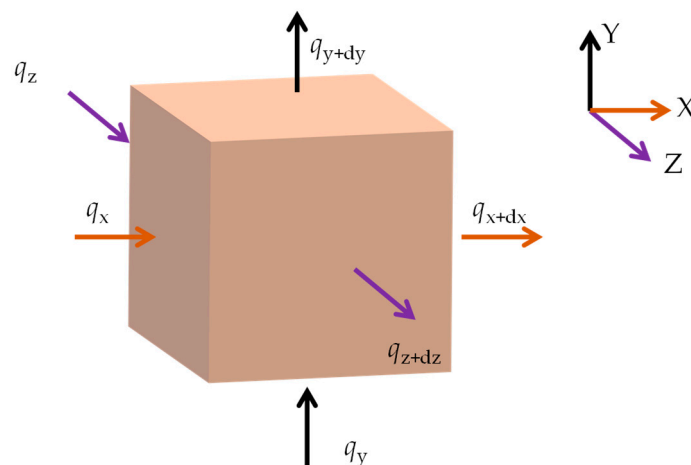


Figure 1. Schematic diagram of heat conduction in the microunit.

2.2.2. Transient Temperature Model

The temperature of the bottom hole fluid during production surpasses the reservoir temperature at an equivalent depth, leading to continuous heat transfer to the surrounding environment until thermal equilibrium is achieved. The fluid heat is transferred to the reservoir through the multilayer wall of the casing and cement ring (Figure 2). Based on the heat transfer characteristics, the heat transfer process within the micro-tube section is divided into two distinct steps: gas heat transfer within the wellbore and heat transfer along the surrounding well walls.

To simplify the model, the assumptions outlined in this paper are incorporated:

- (1) The transmission of heat from high-temperature gas to the sulfur layer occurs through thermal convection.
- (2) Heat transfer in the sulfur layer, tubing, casing, and cement takes place through heat conduction.
- (3) The heat transfer in the annulus is characterized by convection and radiation.

The heat transfer process comprises three components: (1) Axial heat conduction generated by the control component; (2) Radial heat conduction between the control components; and (3) Changes in internal energy, such as sulfur scale, the oil sleeve, and the cement ring, which can be more readily determined through a series thermal conductivity structure. The tubing experiences intricate thermal processes, including heat conduction, heat convection, and heat radiation. Therefore, the thermal conductivity of the oil casing and the cement ring, as well as influencing factors such as annular convection and heat conduction, are crucial in determining the total heat transfer coefficient. Additionally, the presence of sulfur scale can impact heat loss.

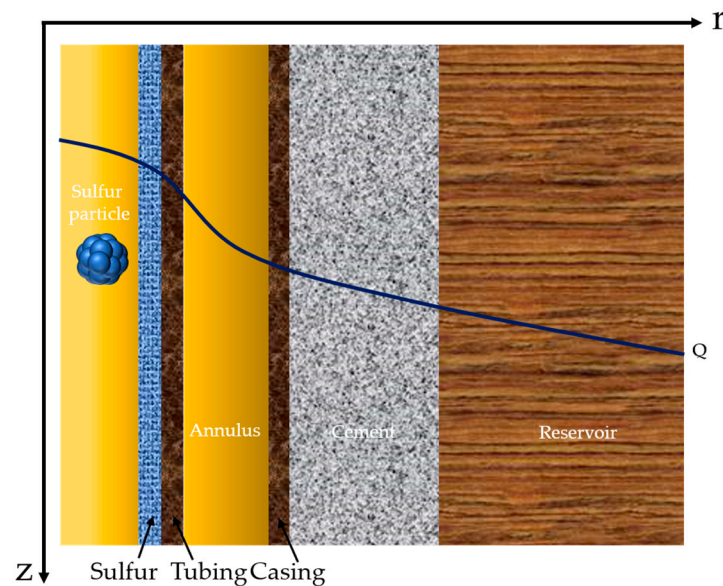


Figure 2. Schematic diagram of heat transfer in HSG well.

The heat transfer of fluid in tubing adheres to the principle of energy conservation. To facilitate the analysis and derivation of the heat transfer in the wellbore, the following hypothesis is proposed based on the flow process of fluid in tubing: (1) The fluid flows statically in a one-dimensional space within the wellbore. (2) The unit controls do not generate any phase change heat within the body, and the temperature of each phase remains constant. The mathematical model can be expressed as follows:

$$\frac{\partial^2 T_s(r, t)}{\partial r^2} + \frac{1}{r} \frac{\partial T_s(r, t)}{\partial r} = \frac{(\rho c)_s}{\lambda_s} \frac{\partial T_s(r, t)}{\partial t} \quad (17)$$

$$\frac{\partial^2 T_{\text{tub}}(r, t)}{\partial r^2} + \frac{1}{r} \frac{\partial T_{\text{tub}}(r, t)}{\partial r} = \frac{(\rho c)_{\text{tub}}}{\lambda_{\text{tub}}} \frac{\partial T_{\text{tub}}(r, t)}{\partial t} \quad (18)$$

$$\frac{\partial^2 T_{\text{cas}}(r, t)}{\partial r^2} + \frac{1}{r} \frac{\partial T_{\text{cas}}(r, t)}{\partial r} = \frac{(\rho c)_{\text{cas}}}{\lambda_{\text{cas}}} \frac{\partial T_{\text{cas}}(r, t)}{\partial t} \quad (19)$$

$$\frac{\partial^2 T_{\text{ann}}(r, t)}{\partial r^2} + \frac{1}{r} \frac{\partial T_{\text{ann}}(r, t)}{\partial r} = \frac{(\rho c)_{\text{ann}}}{(h_c + h_r)_{\text{ann}}} \frac{\partial T_{\text{ann}}(r, t)}{\partial t} \quad (20)$$

$$\frac{\partial^2 T_{\text{cem}}(r, t)}{\partial r^2} + \frac{1}{r} \frac{\partial T_{\text{cem}}(r, t)}{\partial r} = \frac{(\rho c)_{\text{cem}}}{\lambda_{\text{cem}}} \frac{\partial T_{\text{cem}}(r, t)}{\partial \tau} \quad (21)$$

The subscripts *s*, *tub*, *cas*, *ann*, and *cem* represent the sulfur layer, tubing, casing, the annulus, and the cement layer, respectively. It is worth noting that a well may contain multiple casings.

2.3. Wellbore Pressure Model

When the temperature and pressure within the wellbore reach a specific threshold, sulfur particles will precipitate within the wellbore, resulting in a GSTP flow. The pressure drop in this flow can be attributed to three factors: friction, gravity, and acceleration. Due to the higher density of sulfur particles compared to the surrounding fluid, the pressure drop within the wellbore is increased. The formation of a sulfur scale layer on the wellbore surface acts as insulation, reducing heat dissipation to the formation. Additionally, the sulfur scale impacts the flow area by reducing the diameter of the wellbore, resulting in an increased pressure drop and accelerated sulfur deposition. The presence of water in the gas stream can lead to the formation of hydrates, causing blockages in the wellbore that can result in decreased production or complete shutdown. It is imperative to implement proactive preventive and control measures to mitigate production losses and ensure safety.

Due to the significant disparity in dimensions between the length and diameter of the wellbore, the flow of HSG within the wellbore is regarded as a one-dimensional issue. An analysis diagram depicting the microunit is illustrated in Figure 3.

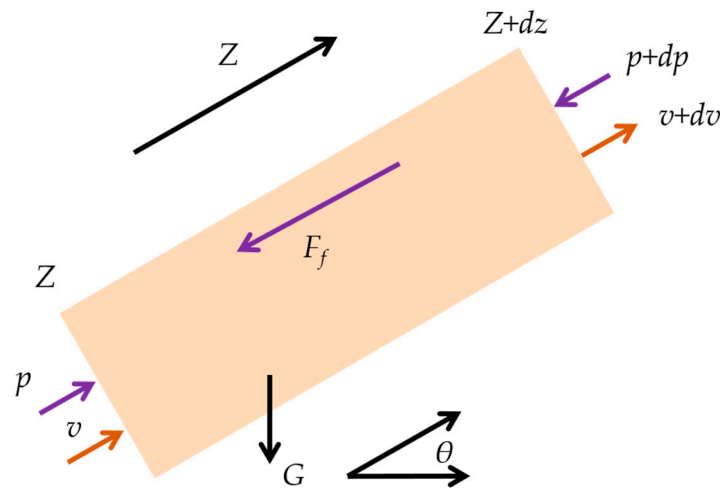


Figure 3. Schematic diagram of gas migration in the microunit.

The external forces acting on the microunit include gravity G , the pressure differential Δp , and frictional resistance F_f .

$$G = -\rho g A dz \sin \theta \quad (22)$$

$$\Delta p = pA - (p + dp)A = -dpA \quad (23)$$

$$F_f = -f \frac{\rho v^2}{2d} dz \quad (24)$$

The change in the momentum of the microunit is $\rho A dz \frac{dv}{dt}$. According to the law of conservation of momentum, we derive

$$\frac{dp}{dz} = \rho g \sin \theta + f \frac{\rho v^2}{2d} + \rho v \frac{dv}{dz} \quad (25)$$

When sulfur particles are precipitated from the HSG, there is a multi-phase flow in the wellbore, so it is necessary to modify the PPPs. The pressure drop can be expressed as Equation (26).

$$\frac{dp_m}{dz} = \rho_m g \sin \theta + f_m \frac{\rho_m v_m^2}{2d} + \rho_m v_m \frac{dv_m}{dz} \quad (26)$$

$$\rho_m = \rho_g (1 - \alpha) + \rho_s \alpha \quad (27)$$

$$v_m = v_g (1 - \alpha) + v_s \alpha \quad (28)$$

$$f_m = f_g (1 - \alpha) + f_s \alpha \quad (29)$$

$$f_s = \frac{27}{F_r^{0.75}} \quad (30)$$

$$F_r = \frac{v_s^2}{g d_s} \quad (31)$$

The friction coefficient is based on the Colebrook model, which is widely used for turbulent flow [39].

$$\frac{1}{\sqrt{f_g}} = -2 \lg \left(\frac{k}{3.7d} + \frac{2.51}{\text{Re} \sqrt{f_g}} \right) \quad (32)$$

$$\text{Re} = \frac{\rho_g v_g d}{\mu_g} \quad (33)$$

2.4. Sulfur Solubility Model

To develop a comprehensive understanding of the precipitation and deposition of elemental sulfur within the wellbore, it is imperative to choose a predictive model for the solubility of elemental sulfur in natural gas. Given that the solubility of elemental sulfur is influenced by variations in pressure and temperature, an examination of the correlation between solubility and these environmental factors is essential for accurate prediction. Thus, an investigation into the interplay between temperature, pressure, and elemental sulfur solubility is warranted. Chrastil proposed a formula based on thermodynamics to predict the solubility of elemental sulfur in HSG [40].

$$C_r = \rho^L \exp \left(\frac{M}{T} + N \right) \quad (34)$$

The area under investigation in this study is situated within Sichuan Province, China. Recent research findings suggest that the proposed prediction model provides a more precise description of sulfur deposition [41]. Utilizing this model, predictive charts illustrating sulfur deposition under varying temperature and pressure conditions can be generated.

$$C_r = \left(\frac{28.96 \gamma_g p}{ZRT} \right)^{-0.0141T + 9.8917} \exp \left(\frac{-813.69}{T} - 12.71 \right) \quad (35)$$

2.5. Initial Conditions and Boundary Conditions

2.5.1. Initial Conditions

At the onset of gas well production, a formation heat balance state is established, with both the wellbore temperature and formation temperature conforming to the linear geothermal gradient.

$$T_i = T_0 + az \quad (36)$$

2.5.2. Boundary Conditions

The formation temperature away from the wellbore is the original formation temperature.

$$T|_{r \rightarrow \infty} = T_i \quad (37)$$

2.6. Numerical Methods

In previous studies, a semi-analytical model was employed to address wellbore temperature [42]. Given the complexity of a numerical model involving multiple partial differential equations for the wellbore-to-formation heat transfer and the necessity for temporal convergence, the fully implicit finite difference method was utilized to resolve these issues.

The temperature field model is governed by a second-order partial differential equation, which is discretized in both the temporal and spatial domains. The resulting discrete formulation of the differential equation is achieved by aggregating the temperature terms at the corresponding spatial and temporal nodes. The resulting system of algebraic equations to be solved is constructed by organizing the temperature variables radially from the wellbore center to the formation, longitudinally from the wellhead to the bottom, and temporally from a shorter to longer duration. The governing equation employs a first-order upwind scheme for the spatial derivative and a two-point backward difference for the time derivative. The second-order spatial derivative is calculated using a three-point central difference scheme. For Equations (17)–(21), the discrete scheme of the specific partial differential equation is

$$\frac{T_{i+1,j}^n - 2T_{i,j}^n + T_{i-1,j}^n}{\Delta r^2} + \frac{1}{r_i} \frac{T_{i+1,j}^n - T_{i,j}^n}{\Delta r} = \frac{\rho c}{\lambda} \frac{T_{i,j}^n - T_{i,j}^{n-1}}{\Delta t} \quad (38)$$

The wellbore pressure model utilizes an explicit difference scheme, while the spatial derivative of the governing equation is implemented using the first-order upwind scheme.

$$\frac{p_j^n - p_{j-1}^n}{\Delta z} = \rho_m g \sin \theta + f_m \frac{\rho_m v_m^2}{2d} + \rho_m v_m \frac{v_j^n - v_{j-1}^n}{\Delta z} \quad (39)$$

2.7. The Calculation Process

The mining process of HSG wells is significantly influenced by the temperature and pressure within the wellbore, which in turn affects the PPPs of the fluid. This reciprocal relationship necessitates iterative calculations to solve the coupled process. A series of initial values are postulated for calculation, with the resultant value being juxtaposed against the assumed initial value. In the event that the outcome fails to satisfy the precision criteria, the calculated result is designated as the new initial value, and subsequent calculations are conducted until the desired level of accuracy is attained. The calculation procedure necessitates computation from the wellhead to the wellbore's base, encompassing the tubing's interior and the formation. The specific calculation process is shown in Figure 4.

The specific calculation steps are as follows:

- (1) Initiate the program and input the initial parameters, which encompass well structure data, production performance data, physical property data, and the heat transfer coefficient.
- (2) Spatial and temporal discretization of the simulation domain is determined based on the depth and radial orientation of the well.
- (3) Calculate the initial temperature, pressure, and PPPs according to Sections 2.1, 2.4 and 2.5.
- (4) At one time step, the pressure field distribution is first calculated. The pressure is calculated in stages from the wellhead to the bottom:

- Based on the findings outlined in Section 2.4, it is imperative to ascertain the attainment of critical solubility and the subsequent precipitation of sulfur. Should sulfur precipitation occur, the utilization of a multi-phase pressure calculation model is warranted; conversely, if sulfur does not precipitate, the adoption of a single-phase pressure calculation model is recommended.
 - Determine the pressure values P_i and P_{i+1} from Section 2.3. Calculate the PPPs and pressure value P'_{i+1} as outlined in Section 2.1, and compare P_{i+1} with P'_{i+1} to assess compliance with the accuracy requirements. If met, proceed to the subsequent step; if not, substitute the value of P_{i+1} with P'_{i+1} and iterate the aforementioned process until the accuracy requirements are satisfied.
 - When the pressure of the i grid reaches the calculated accuracy, the grid moves down, and the pressure in the next grid is calculated until that of the bottom of the hole is calculated.
- (5) The temperature is calculated from the bottom to the wellhead:
- Determine the temperature of the wellbore in grid i using the methodology outlined in Section 2.3. The precision of this calculation is similar to that of the pressure calculation. Following the completion of the calculation, assess the temperature distribution radially from the tubing to the reservoir.
 - As the pressure in the lower part reaches the predetermined level of accuracy, advance the grid upwards and compute the temperature in the subsequent grid until reaching the wellhead.
- (6) The time step calculation method utilized in steps (4) through (5) should be iteratively applied until all time steps have been computed.
- (7) Save the data and output the calculation results.

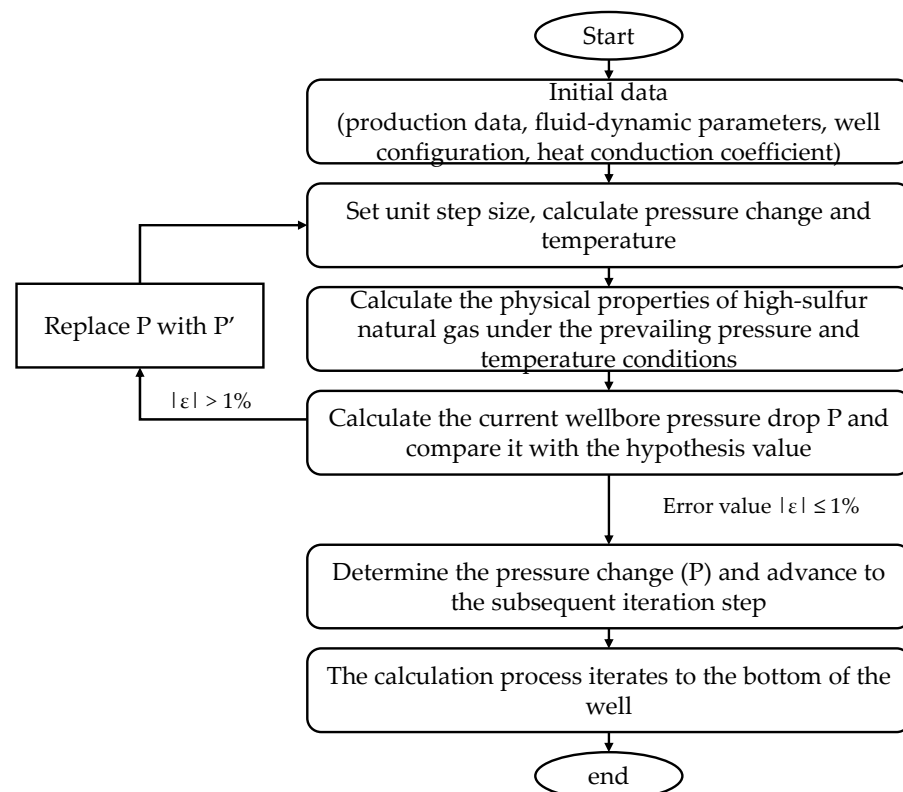


Figure 4. The calculation process.

3. Validation

X Well, located in Sichuan, China, is a hydrogen sulfide gas well characterized by a highly inclined drilling type, a depth of 4860 m, and an HSC of 233.79 mg/m³. The

operators performed well test operations to analyze the wellbore pressure, temperature distribution, reservoir seepage, and productivity characteristics, thereby establishing a technical foundation for the scientific and rational development of the well. The testing procedure is automated using an electronic pressure gauge and is configured to collect data. The experimental test yielded temperature and pressure data, which are presented in Table 3 and Figure 5. The pressure exhibits a linear increase, while the temperature demonstrates rapid changes in the upper region and slower changes in the lower region.

Table 3. Temperature and pressure test result data.

Depth (m)	True Vertical Depth (m)	Pressure (MPa)	Pressure Gradient (MPa/100 m)	Temperature (°C)	Temperature Gradient (°C/100 m)
0.00	0.00	16.620	/	40.78	/
1000.00	999.99	18.584	0.196	68.06	2.73
2000.00	1999.26	20.497	0.191	78.72	1.07
3000.00	2998.94	22.394	0.190	87.73	0.90
3100.00	3097.32	22.580	0.189	88.37	0.65
3250.00	3229.07	21.953	0.257	89.37	0.76

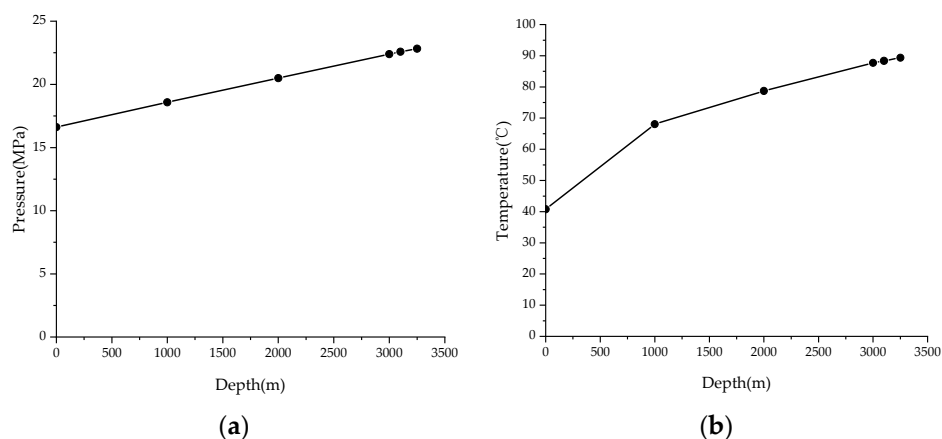


Figure 5. Measured data ((a) pressure; (b) temperature).

A schematic representation of the depth of the structure of well X is illustrated in Figure 6, which comprises three casing layers arranged from innermost to outermost. The production tubing has an outer diameter of 114.3 mm and an inner diameter of 100.54 mm.

A comparison between the test data and calculated data is presented in Figure 7 for temperature and pressure, respectively. The maximum, minimum, and average errors for temperature are 4.94%, 1.29%, and 2.53%, while for pressure, they are 7.07%, 0.2%, and 4.80%. The errors in the pressure calculations are found to be greater than those in the temperature calculations. These results suggest that the model established in this study provides more accurate predictions.

Based on the calculation outlined in the formula for determining sulfur solubility, it was observed that the solubility of elemental sulfur was limited to 0.23 g/cm^3 under the prevailing wellhead pressure and temperature conditions. The declining wellhead pressure in well X prompted the disassembly of the well valve to investigate the potential presence of sulfur deposition. Subsequent experimental analysis revealed that 84.5% of the precipitated substances consisted of sulfur deposits (Table 4). A significant quantity of solid sediment adheres to the inner wall of the import and export pipe, measuring approximately 3–5 mm in thickness and possessing a hardened consistency (Figure 8). Sulfur is consistently adsorbed and accumulated on the pipe wall, transitioning from dispersion to concentration, and subsequently forms a consolidated and thickened layer in a sequential manner from the interior to the exterior. This overall process can be categorized into two distinct stages:

the initial phase involving the aggregation and adsorption of individual particles, followed by the subsequent stage of deposition, consolidation, and thickening.

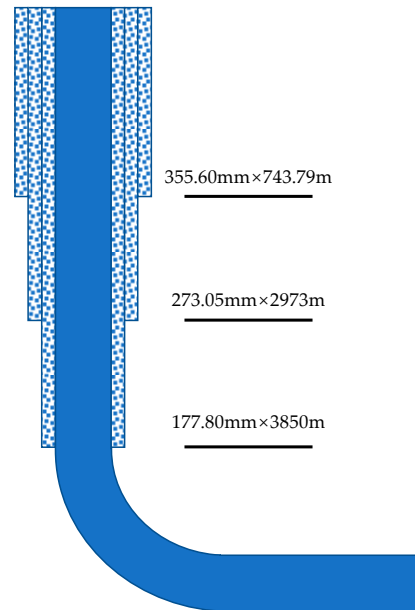


Figure 6. Wellbore structure of well X.

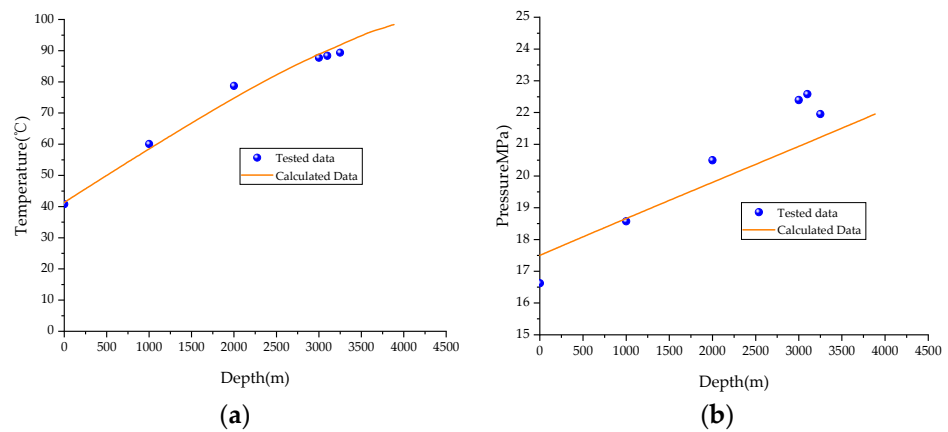


Figure 7. Comparison between calculated data and test data ((a) temperature; (b) pressure).



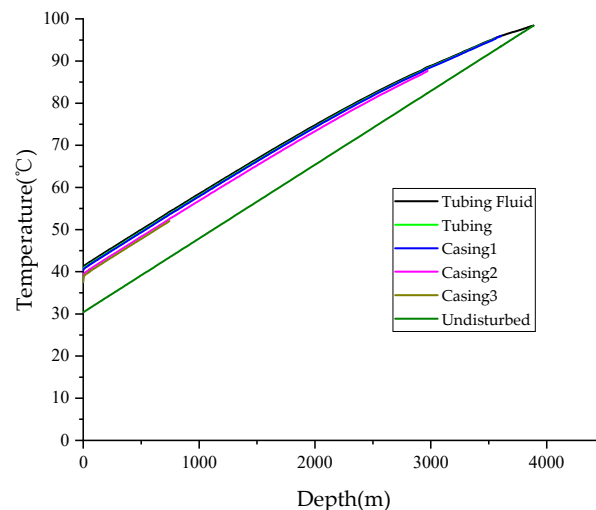
Figure 8. Sulfur deposits in surface pipelines.

Table 4. Test results of components.

Component	Na ₂ O	MgO	Al ₂ O ₃	SiO ₂	P ₂ O ₅	SO ₃	Cl	K ₂ O
Mass ratio	0.0905	0.1089	0.8055	1.6912	0.0174	3.6514	0.0305	0.0828
Component	CaO	Fe ₂ O ₃	NiO	CuO	ZnO	SrO	BaO	S
Mass ratio	0.1676	0.4706	0.0087	0.0154	0.1239	0.0202	8.0479	84.668

4. Discussion

Utilizing the data obtained from well X and employing the model outlined in this study, the temperature profile distribution of the wellbore is computed, as depicted in Figure 9. This analysis enables examination not only of the temperature distribution of the fluid but also of the tubing and casing. The gas travels from the reservoir to the wellbore and subsequently to the surface processing facilities, with a continual decrease in pressure and temperature throughout the entire process. The surface processing stage is characterized by low temperatures and pressures, resulting in minimal solubility of elemental sulfur in the natural gas. Initially, the surface process leads to precipitation and sedimentary blockage, which subsequently progresses to the reservoir of wellbore sulfur deposition blockage.

**Figure 9.** Temperature field.

This section will explore the primary factors influencing the temperature and pressure distribution. The findings of this exploration will elucidate the varying degrees of influence exerted by different factors on temperature and pressure and provide a theoretical basis for the judgment of sulfur deposition.

4.1. Gas Productivity

Variations in gas well production lead to corresponding fluctuations in the distribution of pressure within the well. This study conducted calculations to determine the wellhead temperature and annular flow pressure under three distinct production rates: $60 \times 10^4 \text{ m}^3/\text{d}$, $90 \times 10^4 \text{ m}^3/\text{d}$, and $120 \times 10^4 \text{ m}^3/\text{d}$. The results of these calculations are presented in Figures 10 and 11. The highest recorded wellhead temperature was $49.6 \text{ }^\circ\text{C}$, while the lowest temperature reached $41.3 \text{ }^\circ\text{C}$. As the production levels doubled, there was a corresponding 20.09% increase in the wellhead temperature. The rise in gas production leads to a notable elevation in the wellhead gas temperature. The proximity of gas to the wellhead results in a more pronounced temperature differential among various gas production levels. This phenomenon can be attributed to the heightened heat loss of gas within the tubing, caused by the substantial temperature variance between the gas within the tubing and the reservoir. Additionally, as gas production increases, the fluctuation

in the gas density within the tubing remains minimal, while the difference of pressure is not obvious.

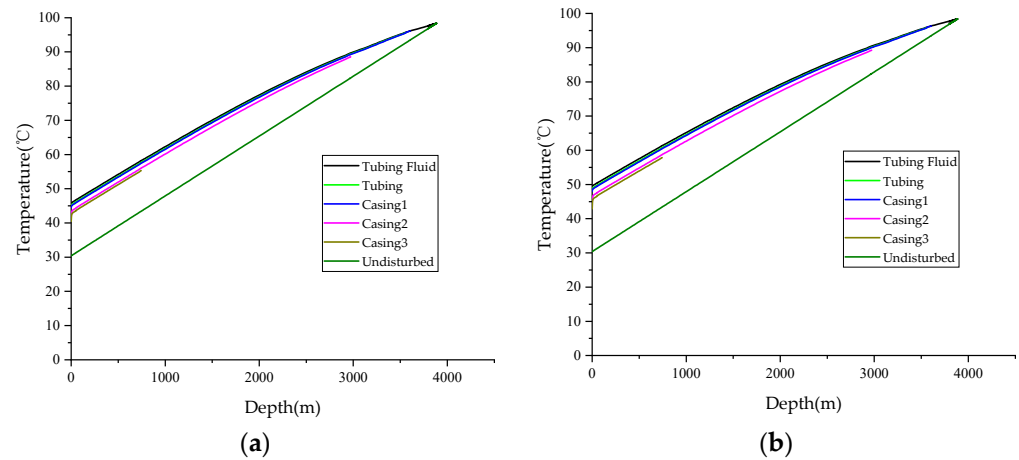


Figure 10. WTD at different gas productivities ((a) $60 \times 10^4 \text{ m}^3/\text{d}$; (b) $120 \times 10^4 \text{ m}^3/\text{d}$).

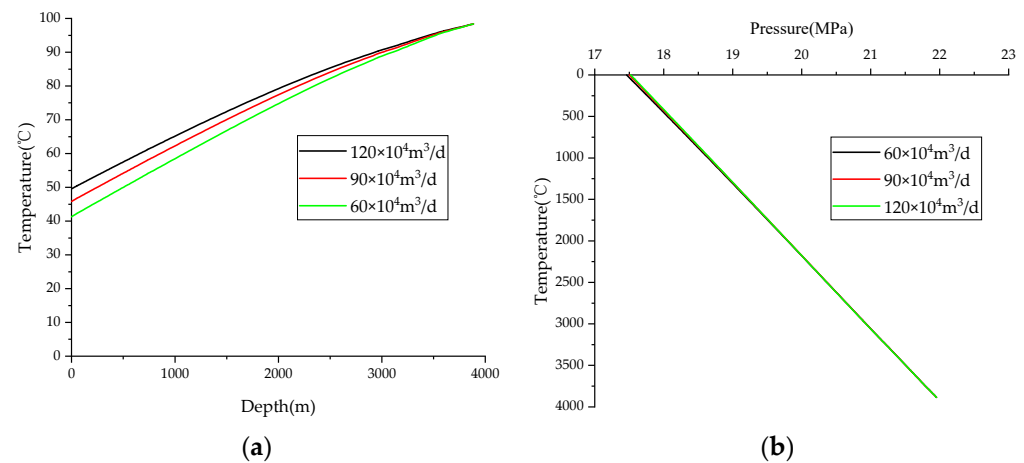


Figure 11. Comparison at different gas productivities ((a) temperature; (b) pressure).

4.2. Sulfur Thickness

The thickness of the sulfur layer was varied at 10 mm, 20 mm, and 30 mm for the purpose of conducting a comparative analysis (Figures 12 and 13). It was observed that the pressure fluctuations at the wellhead were significant, with a maximum pressure of 17.46 MPa and a minimum pressure of 16.90 MPa. When sulfur precipitates in the wellbore, the resulting particles have a very small radius, typically on the nanometer scale. Due to their size and adhesive properties, these particles do not settle at the bottom of the well under the influence of gravity but instead adhere to the walls of the oil pipe. This results in a relatively uniform distribution of sulfur particles, forming a ring-like pattern that gradually thickens to create a layer of sulfur scale. The formation of sulfur on the pipe wall can lead to changes in its surface roughness and diameter, impacting the flow rate, friction resistance, and pressure drop. However, the influence of the sulfur's thickness on the fluid dynamics within the pipe and the temperature field surrounding it is minimal.

4.3. HSC

The HSC was varied at levels of 0%, 20%, and 40% for the purpose of conducting a comparative analysis (Figures 14 and 15). While the temperature differences were minimal across the different HSC levels, there was a noticeable change in pressure. Specifically, the wellhead pressure was measured at 16.0 MPa for a 20% H_2S content and 14.0 MPa for a 40% H_2S content. Higher HSCs were found to result in increased natural gas density.

Consequently, higher HSCs led to more rapid pressure drops, a greater dissolution capacity, and reduced sulfur precipitation. The influence of specific heat capacity on temperature during the precipitation of sulfur particles is comparatively lower, as compared to that of single-phase gas, owing to the reduced solid content.

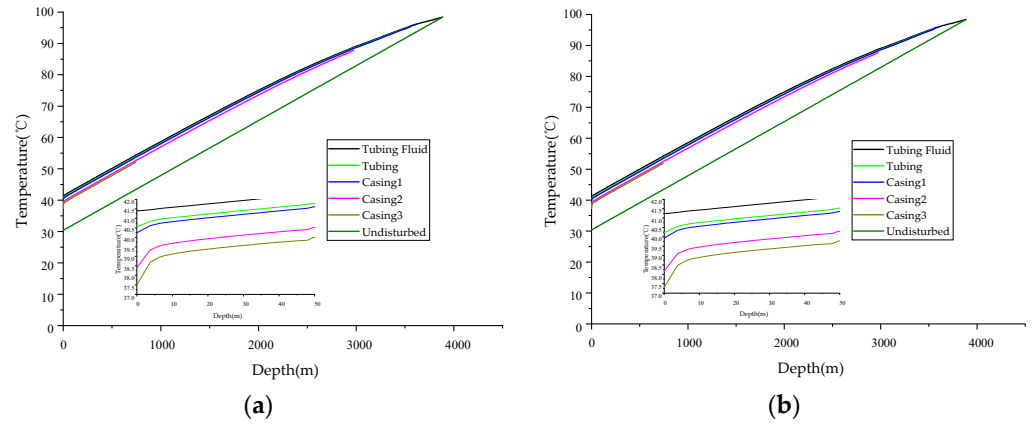


Figure 12. WTD at different sulfur thicknesses ((a) 20 mm; (b) 30 mm).

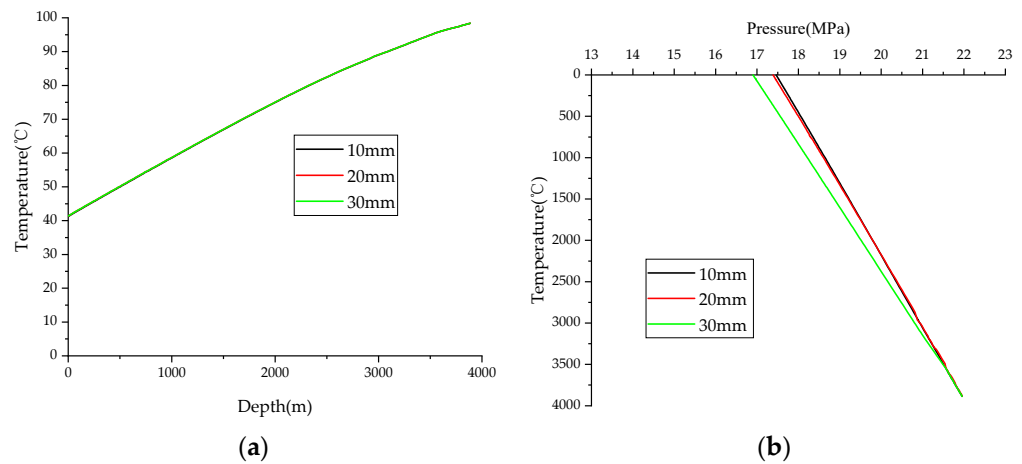


Figure 13. Comparison of results at different sulfur thicknesses ((a) temperature; (b) pressure).

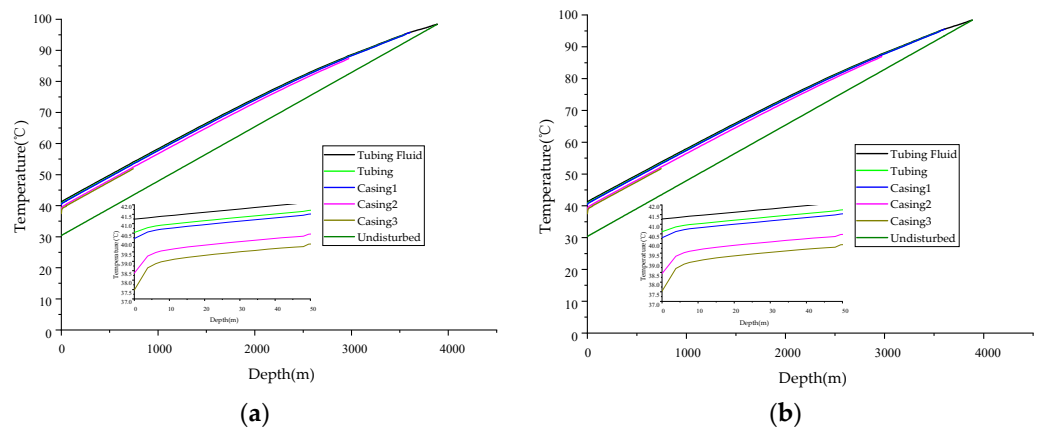


Figure 14. WTD at different HSCs ((a) 20%; (b) 40%).

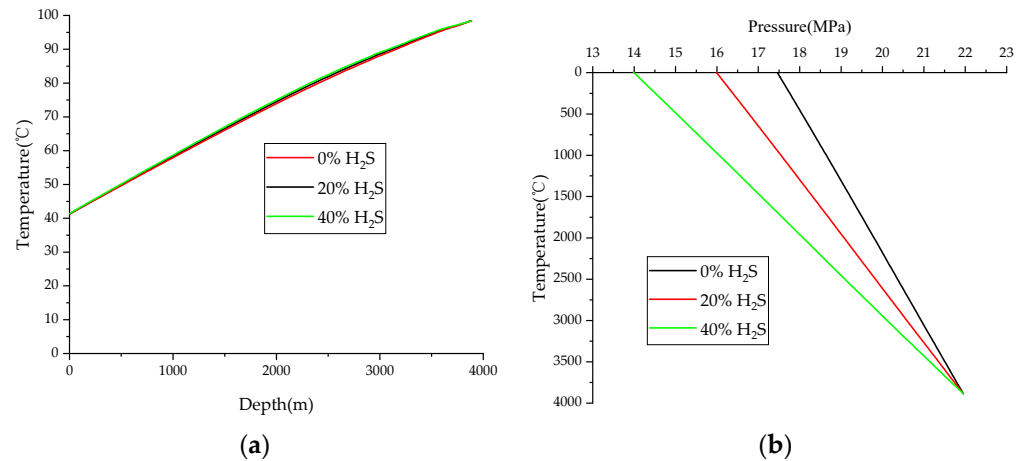


Figure 15. Comparison at different HSCs ((a) temperature; (b) pressure).

4.4. Reservoir Pressure

During the intermediate and advanced stages of development in an HSG field, continuous gas extraction leads to diminished reservoir energy and a decline in reservoir pressure. Consequently, the pressure within the wellbore also diminishes significantly, exacerbating sulfur deposition and posing significant production challenges. Comparative analysis was conducted with the reservoir pressures set at 21.9 MPa, 15 MPa, and 10 MPa, respectively (Figures 16 and 17). With a consistent temperature gradient, minimal change is observed in the temperature of the wellbore fluid and the surrounding wellhead wall. However, a more pronounced change is evident in the wellhead pressure. When the reservoir pressure is at 10 MPa, the wellhead pressure is only 7.9 MPa, significantly lower than the pressure required for sulfur deposition. Consequently, sulfur deposition may extend from the wellhead to the wellbore bottom and potentially infiltrate the reservoir. This poses a significant challenge in mitigating sulfur deposits, ultimately leading to decreased production efficiency and hastening the abandonment of the well.

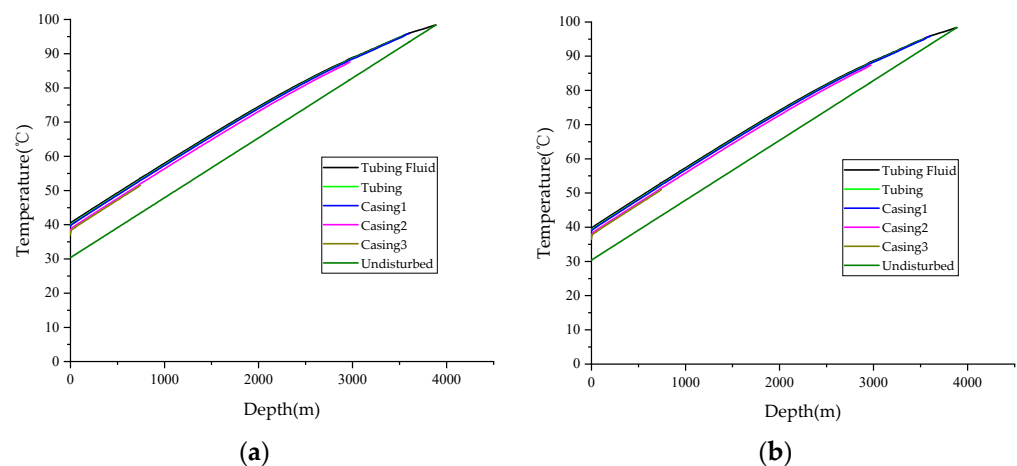


Figure 16. WTD at different reservoir pressures ((a) 15.0 MPa; (b) 10.0 MPa).

4.5. Reservoir Temperature

Variation in the reservoir temperature gradient will exert a notable influence on the spatial distribution of the wellbore temperature, with the reservoir temperatures set at 140/120/100 °C for comparative purposes (Figures 18 and 19). A greater reservoir temperature gradient correlates with elevated wellhead temperatures and correspondingly higher temperatures along the surrounding well walls. The decrease in the wellhead temperature is attributed to the substantial temperature variance in the lower section of the wellbore, leading to heightened heat dissipation, as opposed to the minimal temperature

differential between the upper wellbore and the surrounding strata, resulting in reduced heat dissipation. Additionally, the temperature gradient plays a crucial role in influencing the pressure within the wellbore, as alterations in temperature can impact gas density, consequently affecting the pressure gradient. With an increase in the wellhead temperature, the wellhead pressure increases correspondingly.

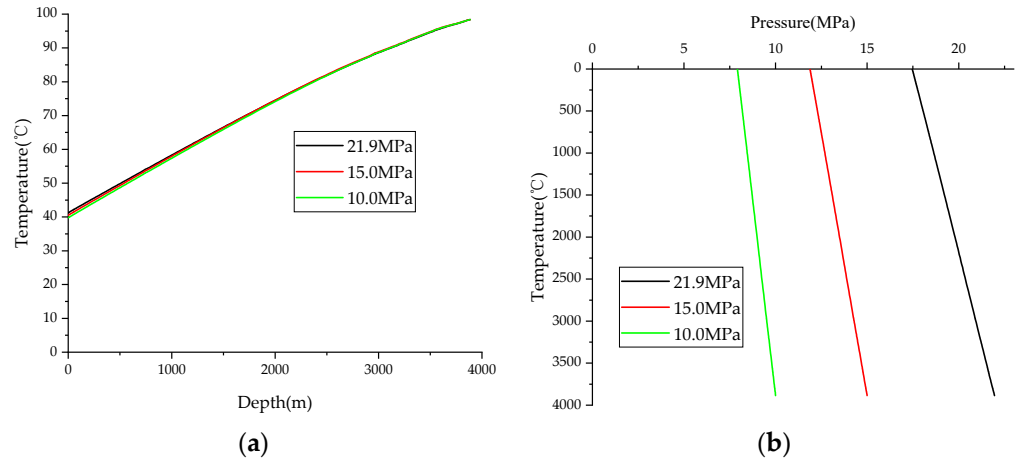


Figure 17. Comparison at different reservoir pressures ((a) temperature; (b) pressure).

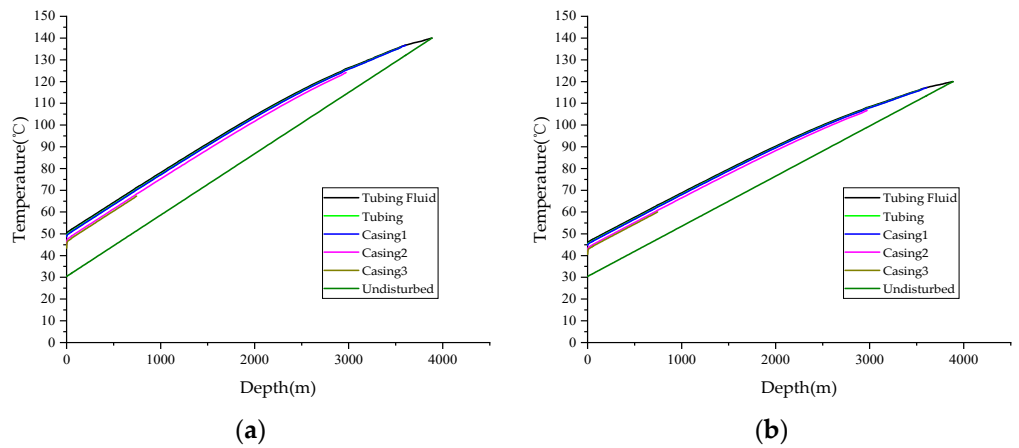


Figure 18. WTD at different reservoir temperatures ((a) 140 °C; (b) 120 °C).

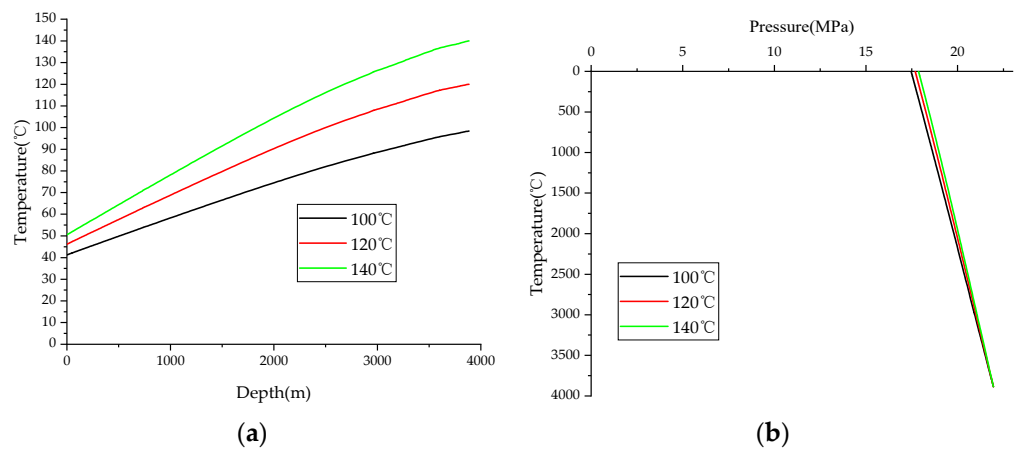


Figure 19. Comparison at different reservoir temperatures ((a) temperature; (b) pressure).

5. Conclusions

- (1) A temperature field prediction model incorporating sulfur deposition was developed, emphasizing variations in the PPPs of hydrogen-sulfide-containing gas and the corresponding modified model. The pressure model employed a GSTP flow approach, while the sulfur solubility prediction model selected a theoretical model tailored to the specific target block.
- (2) The accuracy of the calculation model is validated through comparison with field-measured data, revealing an error of 2.53% in the temperature calculations and 4.80% in the pressure calculations. The results demonstrate a high level of agreement, indicating that the model is suitable for predicting wellbore temperatures in HSG wells.
- (3) The production of the HSG well has a notable impact on temperature. Specifically, a 20.09% increase in the wellhead temperature is observed when comparing a gas production rate of $120 \times 10^4 \text{ m}^3/\text{d}$ to that of $60 \times 10^4 \text{ m}^3/\text{d}$. The thickness of the sulfur scale within the wellbore influences the flow rate, subsequently leading to a decrease in wellhead pressure.
- (4) An elevation in the hydrogen sulfide concentration correlates with an increase in the density of natural gas, thereby causing a more rapid decline in pressure. This reduction in reservoir pressure and temperature will subsequently lower the wellbore pressure and temperature, impeding the removal of sulfur deposits at the well bottom and accelerating a decrease in the productivity of HSG wells.
- (5) This paper primarily examines a prediction model for temperature fields, without delving extensively into the specific locations and mechanisms of sulfur deposition under varying temperature conditions. Future research may explore these aspects further, enabling decision-makers to implement tailored strategies for sulfur deposition removal.

Author Contributions: Conceptualization, Q.F. and J.H.; methodology, Q.F.; validation, Y.W. and H.P.; investigation, H.L.; writing—original draft preparation, J.H.; writing—review and editing, Q.F.; visualization, H.L.; supervision, H.R. All authors have read and agreed to the published version of the manuscript.

Funding: This research was funded by “application field test technology of sulfur deposition control technology in Tieshanpo gas field”, grant number XNS JS2023-90.

Data Availability Statement: The data presented in this study are unavailable due to privacy.

Conflicts of Interest: Authors Yang Wang, Hong Pan, Hongming Ren were employed by the PetroChina Southwest Oil and Gas field Company. The remaining authors declare that the research was conducted in the absence of any commercial or financial relationships that could be construed as a potential conflict of interest. The company had no role in the design of the study; in the collection, analyses, or interpretation of data; in the writing of the manuscript, or in the decision to publish the results.

Abbreviations

HSG	high-sulfur gas
GSTP	gas–solid two-phase
WTD	wellbore temperature distribution
PPP	physical property parameter
HSC	hydrogen sulfide content
Z	Deviation coefficient
P_r	Pseudo pressure
T_r	Pseudo pressure
ϵ	Correction coefficient
M	The sum of the mole fractions of H_2S and CO_2 in the system
N	The mole fraction of H_2S in the system

T_{ci}	Critical temperature, K
p_{ci}	Critical pressure, Pa
T'_{ci}	Corrected critical temperature, K
p'_{ci}	Corrected critical pressure, Pa
γ_g	Relative density of natural gas
$\mu_{H_2S}, \mu_{CO_2}, \mu_{N_2}$	Viscosity correction values for H ₂ S, CO ₂ , and N ₂ , respectively, mPa·s
H_2S, CO_2, N_2	Molar content in the gas mixture, %
λ	Thermal conductivity coefficient, W/(m·K)
T	Temperature, K
r	Distance from the center of the tubing, m
ρ_c	Heat capacity per unit volume, J/(m ³ ·K)
t	Time, s
λ	Heat transfer coefficient, w/(m·K)
h_c	Heat transfer coefficients of heat convection, w/(m·K)
h_r	Heat transfer coefficients of heat radiation, w/(m·K)
α	Content of sulfur particles
ρ_s	Densities of sulfur particles, kg/m ³
ρ_g	Densities of gas, kg/m ³
v_s	Velocity of the solid sulfur particle, m/s
d_s	Diameter of the sulfur particle, m
v_g	Speed of the gas, m/s
d	Inner diameter of the tubing, m
μ_g	Viscosity of the gas, mPa·s
T_i	Initial reservoir temperature at depth z , K
T_0	Wellhead temperature, K
a	Temperature gradient, K/m
z	Depth, m

References

- Zhang, N.; Zhang, Z.; Rui, Z.; Li, J.; Zhang, C.; Zhang, Q.; Zhao, W.; Patil, S. Comprehensive risk assessment of high sulfur-containing gas well. *J. Petrol. Sci. Eng.* **2018**, *170*, 888–897. [\[CrossRef\]](#)
- Liu, W.; Huang, X.; Zhang, L.; He, J.; Cen, X. Analysis of sulfur deposition for high-sulfur gas reservoirs. *Petrol. Sci. Technol.* **2022**, *40*, 1716–1734. [\[CrossRef\]](#)
- Bemani, A.; Baghban, A.; Mohammadi, A.H. An insight into the modeling of sulfur content of sour gases in supercritical region. *J. Petrol. Sci. Eng.* **2020**, *184*, 106459. [\[CrossRef\]](#)
- Xu, Z.; Gu, S.; Zeng, D.; Sun, B.; Xue, L. Numerical simulation of sulfur deposit with particle release. *Energies* **2020**, *13*, 1522. [\[CrossRef\]](#)
- Piemjaiswang, R.; Khaisri, S.; Sema, T.; Chalermisinsuwan, B.; Nimmanterdwong, P. Performance of Data Segmentation ANN Model for Elemental Sulfur Solubility Prediction in Natural Gas Transportation Pipeline. In Proceedings of the 15th International Conference on Computer and Automation Engineering (ICCAE), Sydney, Australia, 3–5 March 2023.
- Sun, C.; Zeng, H.; Luo, J. Unraveling the effects of CO₂ and H₂S on the corrosion behavior of electroless Ni-P coating in CO₂/H₂S/Cl-environments at high temperature and high pressure. *Corros. Sci.* **2019**, *148*, 317–330. [\[CrossRef\]](#)
- Dong, B.; Liu, W.; Cheng, L.; Gong, J.; Wang, Y.; Gao, Y.; Dong, S.; Zhao, Y.; Fan, Y.; Zhang, T. Investigation on mechanical properties and corrosion behavior of rubber for packer in CO₂-H₂S gas well. *Eng. Fail. Anal.* **2021**, *124*, 105364. [\[CrossRef\]](#)
- Ramey, H.J., Jr. Wellbore heat transmission. *J. Pet. Technol.* **1962**, *14*, 427–435. [\[CrossRef\]](#)
- Willhite, G.P. Over-all heat transfer coefficients in steam and hot water injection wells. *J. Pet. Technol.* **1967**, *19*, 607–615. [\[CrossRef\]](#)
- Raymond, L.R. Temperature distribution in a circulating drilling fluid. *J. Pet. Technol.* **1969**, *21*, 333–341. [\[CrossRef\]](#)
- Eickmeier, J.R.; Ersoy, D.; Ramey, H.J. Wellbore temperatures and heat losses during production or injection operations. *J. Can. Pet. Technol.* **1970**, *9*, 115–121. [\[CrossRef\]](#)
- You, J.; Rahnema, H.; McMillan, M.D. Numerical modeling of unsteady-state wellbore heat transmission. *J. Nat. Gas. Sci. Eng.* **2016**, *34*, 1062–1076. [\[CrossRef\]](#)
- Dong, W.; Shen, R.; Liang, Q. Model calculations and factors affecting wellbore temperatures during SRV fracturing. *Arab. J. Sci. Eng.* **2018**, *43*, 6475–6480. [\[CrossRef\]](#)
- Hasan, A.R.; Kabir, C.S. Aspects of wellbore heat transfer during two-phase flow. *Spe Prod. Facil.* **1994**, *9*, 211–216. [\[CrossRef\]](#)
- Kabir, C.S.; Hasan, A.R.; Jordan, D.L.; Wang, X. A wellbore/reservoir simulator for testing gas wells in high-temperature reservoirs. *Spe Form. Eval.* **1996**, *11*, 128–134. [\[CrossRef\]](#)
- Hasan, A.R.; Kabir, C.S.; Wang, X. Wellbore two-phase flow and heat transfer during transient testing. *Spe J.* **1998**, *3*, 174–180. [\[CrossRef\]](#)

17. Wang, Y.; Ye, J.; Wu, S. A prediction model of wellbore temperature and pressure distribution in hydrocarbon gas injection well, In Proceedings of 5th International Workshop on Renewable Energy and Development, Chengdu, China, 23–25 April 2021.
18. Sun, W.; Wei, N.; Zhao, J.; Zhou, S.; Zhang, L.; Li, Q.; Jiang, L.; Zhang, Y.; Li, H.; Xu, H. Wellbore temperature and pressure field in deep-water drilling and the applications in prediction of hydrate formation region. *Front. Energy Res.* **2021**, *9*, 696392. [[CrossRef](#)]
19. Zheng, J.; Dou, Y.; Li, Z.; Yan, X.; Zhang, Y.; Bi, C. Investigation and application of wellbore temperature and pressure field coupling with gas–liquid two-phase flowing. *J. Pet. Explor. Prod. Technol.* **2022**, *12*, 753–762. [[CrossRef](#)]
20. An, J.; Li, J.; Huang, H.; Liu, G.; Chen, S.; Zhang, G. Numerical study of temperature–pressure coupling model for the horizontal well with a slim hole. *Energy Sci. Eng.* **2023**, *11*, 1060–1079. [[CrossRef](#)]
21. Chen, X.; Wang, S.; He, M.; Xu, M. A comprehensive prediction model of drilling wellbore temperature variation mechanism under deepwater high temperature and high pressure. *Ocean. Eng.* **2024**, *296*, 117063. [[CrossRef](#)]
22. Brunner, E.; Place, M.C., Jr.; Woll, W.H. Sulfur solubility in sour gas. *J. Pet. Technol.* **1988**, *40*, 1587–1592. [[CrossRef](#)]
23. Serin, J.; Jay, S.; Cézac, P.; Contamine, F.; Mercadier, J.; Arrabie, C.; Legros-Adrian, J. Experimental studies of solubility of elemental sulphur in supercritical carbon dioxide. *J. Supercrit. Fluids* **2010**, *53*, 12–16. [[CrossRef](#)]
24. Cloarec, E.; Serin, J.; Cézac, P.; Contamine, F.; Mercadier, J.; Louvat, A.; Casola Lopez, A.; Van Caneghem, P.; Forster, R.; Kim, U. Experimental studies of solubility of elemental sulfur in methane at 363.15 K for pressure ranging from (4 to 25) MPa. *J. Chem. Eng. Data* **2012**, *57*, 1222–1225. [[CrossRef](#)]
25. Yang, X.F.; Huang, X.P.; Zhong, B. Experimental test and calculation methods of elemental sulfur solubility in high sulfur content gas. *Nat. Gas. Geosci.* **2009**, *20*, 416.
26. Guo, X.; Wang, Q. A new prediction model of elemental sulfur solubility in sour gas mixtures. *J. Nat. Gas. Sci. Eng.* **2016**, *31*, 98–107. [[CrossRef](#)]
27. Wang, Q.; Guo, X.; Leng, R. In-depth study on the solubility of elemental sulfur in sour gas mixtures based on the Chrastil’s association model. *Petroleum* **2016**, *2*, 425–434. [[CrossRef](#)]
28. Karan, K.; Heidemann, R.A.; Behie, L.A. Sulfur solubility in sour gas: Predictions with an equation of state model. *Ind. Eng. Chem. Res.* **1998**, *37*, 1679–1684. [[CrossRef](#)]
29. Wei, Y.; Wang, L.; Yang, Y.; Wen, L.; Huo, X.; Zhang, L.; Yang, M. Molecular mechanism in the solubility reduction of elemental sulfur in H₂S/CH₄ mixtures: A molecular modeling study. *Fluid. Phase Equilib* **2023**, *569*, 113764. [[CrossRef](#)]
30. Heidemann, R.A.; Phoenix, A.V.; Karan, K.; Behie, L.A. A chemical equilibrium equation of state model for elemental sulfur and sulfur-containing fluids. *Ind. Eng. Chem. Res.* **2001**, *40*, 2160–2167. [[CrossRef](#)]
31. Kadoura, A.; Salama, A.; Sun, S.; Sherik, A. An NPT monte carlo molecular simulation-based approach to investigate solid-vapor equilibrium: Application to elemental sulfur-H₂S system. *Procedia Comput. Sci.* **2013**, *18*, 2109–2116. [[CrossRef](#)]
32. ZareNezhad, B.; Aminian, A. Predicting the sulfur precipitation phenomena during the production of sour natural gas by using an artificial neural network. *Petrol. Sci. Technol.* **2011**, *29*, 401–410. [[CrossRef](#)]
33. Mehrpooya, M.; Mohammadi, A.H.; Richon, D. Extension of an artificial neural network algorithm for estimating sulfur content of sour gases at elevated temperatures and pressures. *Ind. Eng. Chem. Res.* **2010**, *49*, 439–442. [[CrossRef](#)]
34. Dranchuk, P.M.; Purvis, R.A.; Robinson, D.B. Computer calculation of natural gas compressibility factors using the Standing and Katz correlation. In Proceedings of the Annual Technical Meeting, Edmonton, AB, Canada, 7–11 May 1973.
35. Wichert, E.; Aziz, K. Calculate Zs for sour gases. *Hydrocarb. Process.* **1972**, *51*, 119.
36. Dempsey, J.R. Computer routine treats gas viscosity as a variable. *Oil Gas J.* **1965**, *63*, 141–143.
37. Standing, M.B. Volumetric and phase behavior of oil field hydrocarbon systems. In *Society of Petroleum Engineers of AIME; Society of Petroleum Engineers of AIME: Wilkes-Barre, PA, USA*, 1952.
38. Shuai, X.; Meisen, A. New correlations predict physical properties of elemental sulfur. *Oil Gas J.* **1995**, *93*, 116529.
39. Colebrook, C.F.; Blench, T.; Chatley, H.; Essex, E.H.; Finnicome, J.R.; Lacey, G.; Williamson, J.; Macdonald, G.G. Correspondence. turbulent flow in pipes, with particular reference to the transition region between the smooth and rough pipe laws. *J. Inst. Civ. Eng.* **1939**, *12*, 393–422. [[CrossRef](#)]
40. Chrastil, J. Solubility of solids and liquids in supercritical gases. *J. Phys. Chem.* **1982**, *86*, 3016–3021. [[CrossRef](#)]
41. FU, D. Dynamic Characteristics and Countermeasures of Sulfur Plugging in Gas Wells of Puguang Gas Field. *J. Southwest Pet. Univ.* **2023**, *45*, 119–130.
42. Guo, X.; Wang, P.; Ma, J.; Jia, C. Numerical Simulation of Sulfur Deposition in Wellbore of Sour-Gas Reservoir. *Processes* **2022**, *10*, 1743. [[CrossRef](#)]

Disclaimer/Publisher’s Note: The statements, opinions and data contained in all publications are solely those of the individual author(s) and contributor(s) and not of MDPI and/or the editor(s). MDPI and/or the editor(s) disclaim responsibility for any injury to people or property resulting from any ideas, methods, instructions or products referred to in the content.